MATEXPERT: DECOMPOSING MATERIALS DISCOVERY BY MIMICKING HUMAN EXPERTS

Anonymous authors
Paper under double-blind review

ABSTRACT

Material discovery is a critical research area with profound implications for various industries. In this work, we introduce *MatExpert*, a novel framework that leverages Large Language Models (LLMs) and contrastive learning to accelerate the discovery and design of new solid-state materials. Inspired by the workflow of human materials design experts, our approach integrates three key stages: retrieval, transition, and generation. First, in the retrieval stage, MatExpert identifies an existing material that closely matches the desired criteria. Second, in the transition stage, MatExpert outlines the necessary modifications to transform this material formulation to meet specific requirements outlined by the initial user query. Third, in the generation state, MatExpert performs detailed computations and structural generation to create new materials based on the provided information. Our experimental results demonstrate that MatExpert outperforms state-of-the-art methods in material generation tasks, achieving superior performance across various metrics including validity, distribution, and stability. As such, MatExpert represents a meaningful advancement in computational material discovery using langauge-based generative models.

1 INTRODUCTION

The discovery and design of new materials are central challenges in modern materials science, driven by the need for materials with tailored properties for applications in energy, electronics, and catalysis. Traditional methods for material discovery, such as high-throughput experiments and density functional theory (DFT) simulations, are computationally expensive and often require significant domain expertise to achieve accurate predictions (Miret et al., 2024). Recent advancements in artificial intelligence (AI), particularly large language models (LLMs), have opened new possibilities for automating and accelerating the materials design process (Miret & Krishnan, 2024; Jablonka et al., 2024; Song et al., 2023a;b; Zhang et al., 2024; Ramos et al., 2024).

LLMs such as GPT-4 OpenAI (2023) have demonstrated remarkable success in natural language processing tasks and have shown potential for application in scientific problems beyond language, including chemistry and materials science Flam-Shepherd & Aspuru-Guzik (2023); Gruver et al. (2024); Schilling-Wilhelmi et al. (2024); Mirza et al. (2024); Delétang et al. (2023). For example, LLMs have been used to generate molecular structures Gruver et al. (2024) and predict material properties from textual descriptions Alampara et al. (2024). In the context of material generation, models like Crystal Diffusion Variational Autoencoders (CDVAE) Xie et al. (2022b), as well as fine-tuned LLMs such as LLaMA-2 Gruver et al. (2024), CrystaLLM Antunes et al. (2023), and LM-AC/LM-CH, have made significant progress in generating crystal structures directly from Crystallographic Information Files (CIFs) Antunes et al. (2023). Together, these models aim to accelerate materials design by predicting stable structures and optimizing key properties, such as energy above hull for stability Riebesell et al. (2023).

Despite the significant progress made in applying AI models to materials science, current methods for material generation still face critical limitations Miret & Krishnan (2024); Alampara et al. (2024); Mirza et al. (2024). Most approaches generate material structures in a single step, often resulting in static outputs that lack the flexibility for iterative refinement and optimization based on intermediate feedback. Moreover, these models struggle to integrate multimodal data—such as textual descriptions of desired properties and structural information like atomic coordinates from Crystallographic

Information Files (CIFs)—in a meaningful and cohesive way. Consequently, they fall short of replicating the complex, reasoning-driven processes employed by human experts, limiting their ability to generate materials that meet specific target properties.

In contrast to AI models, human experts follow a methodical, multi-step process when designing new materials. They begin by identifying an existing material with properties closely matching the desired specifications. From there, they apply a series of logical modifications—such as altering atomic arrangements or chemical compositions—to iteratively refine the material. Only after extensive refinement do they finalize the structural details, ensuring that the material is both feasible and aligned with the target properties.

To overcome the limitations of current models, we propose *MatExpert*, a framework that mimics this expert-driven workflow by breaking down the material generation process into three stages: retrieval, transition, and generation. Using a text-structure retrieval approach combined with chain-of-thought reasoning Wei et al. (2022), *MatExpert* can iteratively refine materials based on intermediate feedback, leading to more accurate and interpretable material designs that meet desired specifications.

To comprehensively assess the performance of *MatExpert*, we assembled a large-scale dataset from the NOMAD database Scheidgen et al. (2023), which contains a total of $2,886,120$ materials. This extensive evaluation on a large-scale testbed demonstrates the robustness and generalizability of *MatExpert* in addressing real-world materials discovery challenges.

Concretely, our paper makes the following contributions:

1. We propose *MatExpert*, a novel framework that mimics the expert-driven workflow for material discovery by decomposing the generation process into three stages: retrieval, transition, and generation. By leveraging a text-structure retrieval mechanism and a chain-of-thought reasoning approach, *MatExpert* enables the design of accurate and interpretable materials.
2. We curated a large-scale dataset from the NOMAD Scheidgen et al. (2023) database, which serves as a comprehensive testbed for evaluating *MatExpert* across diverse material compositions. We will publicly release the datasets and source codes upon publication.
3. We conducted extensive experiments on both the Material Project Jain et al. (2013) and the curated NOMAD datasets. Our results demonstrate that *MatExpert* significantly outperforms state-of-the-art baseline methods in material generation, showcasing its effectiveness and generalizability.

2 RELATED WORK

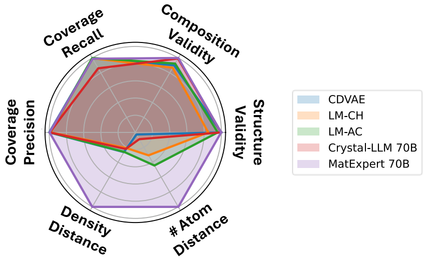

Figure 1: MatExpert achieves remarkable performance on all metrics compared with baselines, especially metrics of distances. See Table 1 for details.

The use of AI and large language models (LLMs) in materials science has gained traction as a means to accelerate material discovery, which traditionally relies on computationally intensive methods like DFT simulations Duval et al. (2023); Govindarajan et al. (2024). Miret & Krishnan (2024) provide an extensive review of the limitations of current LLMs in materials science, particularly their inability to handle multi-modal data and iteratively refine structures based on feedback.

Early work, such as the Crystal Diffusion Variational Autoencoder (CDVAE) Xie et al. (2022b), generated crystal structures by incorporating physical stability constraints to produce valid periodic materials. Recent work has expanded on CDVAE's approach by exploring alternative representations for diffusion-based models Jiao et al. (2024); Yang et al. (2024); Zeni et al. (2023), as well as flow-matching models Miller et al. (2024). Further advancements include the fine-tuning of LLMs for materials generation. Gruver et al. (2024) fine-tuned LLaMA-2, improving metastable material generation rates, while CrystaLLM Antunes et al. (2023) employs an autoregressive model trained on CIF files to generate inorganic crystal structures, leveraging Monte Carlo Tree Search for refine-

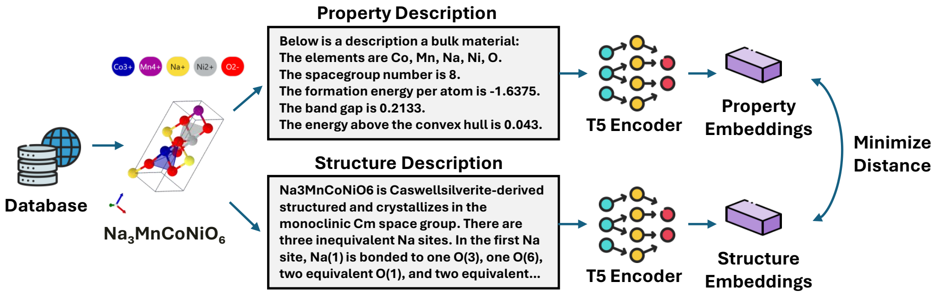

Below is a description a bulk material:
The elements are Co, Mn, Na, Ni, O.
The spacegroup number is 8.
The formation energy per atom is -1.6375.
The band gap is 0.2133.
The energy above the convex hull is 0.043.

Na3MnCoNiO6 is Caswellsilverite-derived structured and crystallizes in the monoclinic Cm space group. There are three inequivalent Na sites. In the first Na site, Na(1) is bonded to one O(3), one O(6), two equivalent O(1), and two equivalent...

Figure 2: We utilize a contrastive learning framework to train two encoders for reference material retrieval. For a given sample material (e.g., $Na_3MnCoNiO_6$), we extract both its property description and structural description using PyMatgen Ong et al. (2013) and Robocrystallographer Ganose & Jain (2019), respectively. The model employs two T5-based encoders Raffel et al. (2020), which are trained to minimize the distance between these two representations.

ment. Flam-Shepherd & Aspuru-Guzik (2023) proposed LM-AC and LM-CH, which explore generating 3D molecular structures directly from CIF, XYZ, and PDB formats, pushing the boundaries of LLM applications in material science. In addition to generative models for materials discovery, as well as the development domain-specific LLMs for diverse language tasks materials science (Song et al., 2023b;a; Xie et al., 2023; Zhang et al., 2024), LLMs are also being used to automate the extraction of structured data from scientific literature, streamlining the creation of datasets for machine learning Hira et al. (2024); Mishra et al. (2024); Schilling-Wilhelmi et al. (2024).

In summary, while LLMs show great promise, challenges remain in integrating multi-modal data and refining material designs iteratively. Most prior work has focused on unconditioned material generation, but current methods lack the ability to iteratively refine and reason like human experts. Our *MatExpert* framework addresses this shortcoming by mimicking an expert-driven workflow, employing multi-stage iterative refinement through retrieval, transition, and generation processes, and achieves remarkable performance compared to state-of-the-art methods, particularly in metrics of distances (see Figure 1).

3 METHODOLOGY

Our *MatExpert* framework simplifies the complex process of material discovery by emulating human experts through three key stages: **retrieval**, **transition**, and **generation**. First, we retrieve a reference material from a database that closely aligns with the desired properties. Next, using a fine-tuned large language model (LLM) with Low-Rank Adaptation (LoRA) Hu et al. (2022), we generate insights on how to modify the reference material to meet the target specifications. Finally, we generate the new material's structure based on the reference and transition steps. The framework employs a T5-based Raffel et al. (2020) model for the retrieval stage and a fine-tuned LLM for the transition and generation stages. A comprehensive illustration of the MatExpert framework pipeline is shown in Figure 3.

3.1 FIRST STAGE: RETRIEVAL

The retrieval stage is the foundational step of our framework, aimed at identifying the material in the database that best matches the desired property description provided by the user.

To bridge the gap between the representation of the desired properties and the relevant material, we apply contrastive learning. Contrastive learning Chen et al. (2020) is a self-supervised method that learns representations by bringing positive pairs closer together while pushing negative pairs farther apart in the embedding space. Contrastive learning was first applied in the domain Radford et al. (2021); Singh et al. (2022), recent works have successfully applied similar methods to domains to materials design, such as molecular Liu et al. (2022) and protein modeling Xu et al. (2023). In the context of material retrieval, we use this method to embed material properties and structures in a shared space, enabling the efficient retrieval of materials that closely match specific queries.

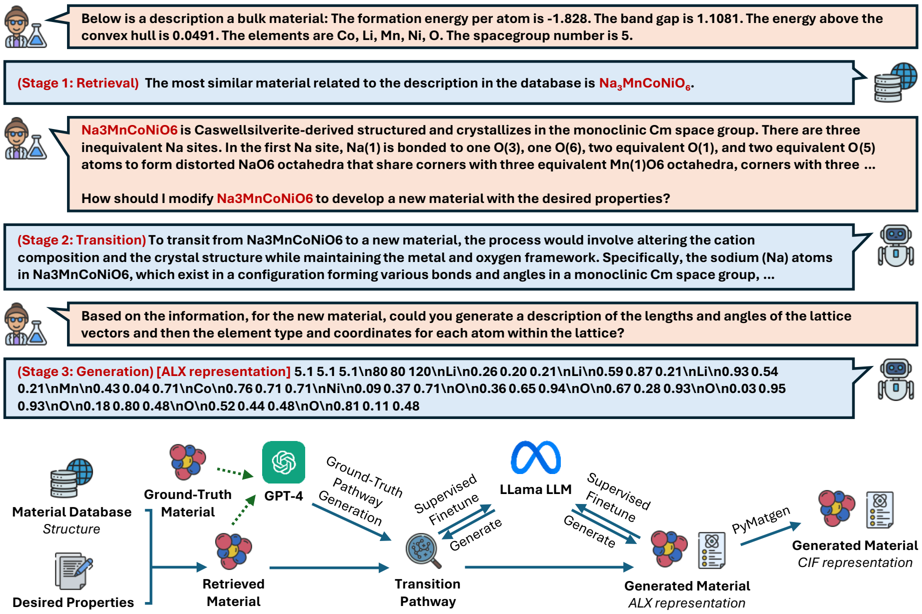

Below is a description a bulk material: The formation energy per atom is -1.828. The band gap is 1.1081. The energy above the convex hull is 0.0491. The elements are Co, Li, Mn, Ni, O. The spacegroup number is 5.

(Stage 1: Retrieval) The most similar material related to the description in the database is $Na_3MnCoNiO_6$.

Na3MnCoNiO6 is Caswellsilverite-derived structured and crystallizes in the monoclinic Cm space group. There are three inequivalent Na sites. In the first Na site, Na(1) is bonded to one O(3), one O(6), two equivalent O(1), and two equivalent O(5) atoms to form distorted NaO6 octahedra that share corners with three equivalent Mn(1)O6 octahedra, corners with three ...

How should I modify Na3MnCoNiO6 to develop a new material with the desired properties?

(Stage 2: Transition) To transit from Na3MnCoNiO6 to a new material, the process would involve altering the cation composition and the crystal structure while maintaining the metal and oxygen framework. Specifically, the sodium (Na) atoms in Na3MnCoNiO6, which exist in a configuration forming various bonds and angles in a monoclinic Cm space group, ...

Based on the information, for the new material, could you generate a description of the lengths and angles of the lattice vectors and then the element type and coordinates for each atom within the lattice?

(Stage 3: Generation) [ALX representation] 5.1 5.1 5.1\n80 80 120\nLi\n0.26 0.20 0.21\nLi\n0.59 0.87 0.21\nLi\n0.93 0.54 0.21\nMn\n0.43 0.04 0.71\nCo\n0.76 0.71 0.71\nNi\n0.09 0.37 0.71\nO\n0.36 0.65 0.94\nO\n0.67 0.28 0.93\nO\n0.03 0.95 0.93\nO\n0.18 0.80 0.48\nO\n0.52 0.44 0.48\nO\n0.81 0.11 0.48

Figure 3: Pipeline of MatExpert: Given a description of the desired material, MatExpert first retrieves the most similar material from the database (e.g., $Na_3MnCoNiO_6$). Next, the LLM provides transition pathways to modify the retrieved material into the desired material (e.g., replacing Na with Li). Finally, the LLM generates the detailed structural information of the desired material ($Li_3MnCoNiO_6$). See Figure 7 for a full case of conditional material generation.

To implement this, we employ a contrastive learning framework (see Figure 2), using two parallel T5-based encoders to process and embed both property and structure descriptions. The property descriptions include key characteristics such as composition, space group number, formation energy, band gap, and energy above hull. Structural descriptions are extracted using RoboCrystallographer, which provides detailed linguistic descriptions of the structure for each material.

The primary objective is to ensure that the embedding of the property description ($\mathbf{q}_i$) is closely aligned with the embedding of the corresponding structure description ($\mathbf{m}_i$), while distinctly separating it from embeddings of other materials ($\mathbf{m}_k$). To quantitatively enforce this alignment, a contrastive loss function is defined as:

$$\mathcal{L} = -\log \frac{\exp(\text{sim}(\mathbf{q}_i, \mathbf{m}_i)/\tau)}{\sum_{k=1}^{N} \exp(\text{sim}(\mathbf{q}_i, \mathbf{m}_k)/\tau)}. \tag{1}$$

Here, $\text{sim}(\mathbf{q}_i, \mathbf{m}_i)$ denotes the cosine similarity between the property and structure embeddings, τ is a temperature parameter that controls the sharpness of the distribution, and N is the size of negative sampling. The output of this stage is the best matching material, which serves as a candidate for further refinement.

3.2 SECOND STAGE: TRANSITION

The transition stage focuses on developing a detailed and viable method for modifying the retrieved material to meet the desired properties. This stage bridges the gap between the existing material and the target material by outlining specific structural or compositional changes required to achieve the desired specifications.

To build a model capable of generating transition pathways that describe how to transform the existing reference material into the desired target material, two key steps are necessary: (1) constructing a training dataset consisting of `<source material, transition pathways, target material>` triples, and (2) fine-tuning a model that can produce `transition pathways` given an `source material` as a reference.

In this stage, we utilize two LLMs in a sequential process. First, during the training phase, we employ GPT-4 to generate ground-truth transition pathways, which provide comprehensive, step-by-step instructions for transforming the retrieved material to meet the target properties. Subsequently, we fine-tune a second, smaller LLM using these ground-truth pathways. In practical applications, including our experiments, this fine-tuned LLM is deployed to generate the potential transition pathways, offering a more efficient solution while maintaining accuracy.

Ground-Truth Pathway Generation with GPT-4: During the training phase, we utilize GPT-4 to generate detailed transition pathways by providing it with carefully designed prompts. These prompts are constructed to ensure that GPT-4 receives all necessary information about both the source material and the target material, enabling it to produce accurate and comprehensive modification pathways. An example template of such a prompt is:

`I have two materials: <formula_source> and <formula_target>. Based on the descriptions and properties of the two materials below, can you summarize the main reasons for the differences in properties when transitioning from <formula_source> to <formula_target>? The description of <formula_source>: <description_source>. The description of <formula_target>: <description_target>.`

Fine-Tuning the Second LLM: The ground-truth transition pathways generated by GPT-4 form the basis for the supervised fine-tuning of a second LLM. This model is trained to learn and replicate the detailed modification steps provided by GPT-4, allowing it to generate potential transition pathways in practical applications. An example prompt template used for fine-tuning is:

`I am looking to design a new material with the following properties: <property_list>. The closest existing material I found in the database is <formula_source>, which has similar properties. Below is the structure description of <formula_source>. \n <description_source> \n How should I modify <formula_source> to develop a new material with the desired properties?`

3.3 THIRD STAGE: GENERATION

The generation stage is focused on producing the CIF (Crystallographic Information File) representation of the predicted material. Specifically, we first generate a detailed description of the lattice vectors and atomic coordinates, which we refer to as the ALX representation. This ALX representation is then automatically converted into CIF format using the `pymatgen` library, which serves as the final output of our framework.

Fine-Tuning: The generation process builds upon the conversation initiated during the earlier stages of the framework. The output from the transition stage serves as input for the generation stage. An additional prompt is introduced to extend the conversation, guiding the model to generate the ALX representation based on the transition pathway provided in the previous stage. The prompt for the generation stage is:

`Based on the information, for the new material, could you generate a description of the lengths and angles of the lattice vectors and then the element type and coordinates for each atom within the lattice?`

ALX Representation: After fine-tuning, the LLM generates the ALX representation for the material based on the transition pathways (as shown in the final response in Figure 3). This representation includes:

- **Lattice Vectors:** The lengths and angles of the lattice vectors that define the unit cell of the material.
- **Atomic Coordinates:** The precise atomic types and their coordinates within the lattice, ensuring that the generated structure aligns with the desired material properties.

Final Output in CIF Format: Once the ALX representation is generated, it is converted into CIF format using the `pymatgen` library. The CIF file contains the complete structural information of the predicted material and serves as the final output of the generation stage. This file can be utilized for further computational studies, experimental validation, or integration into material databases.

4 DATA COLLECTION & PRE-PROCESSING

To rigorously evaluate the performance of *MatExpert*, we assembled a comprehensive dataset from the NOMAD database Scheidgen et al. (2023), utilizing its API. This extensive dataset serves as the large-scale testbed for assessing the capabilities of our framework.

Data Collection from NOMAD NOMAD (Novel Materials Discovery) Scheidgen et al. (2023) is a vast repository of material data, providing access to millions of entries with detailed structural and property information. For our data collection, we applied specific filters to refine the dataset. We excluded materials containing inert elements to focus on those with more active chemical properties, which are of greater interest in materials science research. Additionally, we restricted the dataset to materials whose structures were simulated using the Vienna Ab initio Simulation Package (VASP) Kresse & Hafner (1993), ensuring high-quality computational data. To further improve computational efficiency during training and analysis, we also excluded materials with more than 30 atoms in their original structures.

By applying these filtering criteria, we obtained a dataset of $2,886,120$ materials. This large-scale dataset provides a rich foundation for training and evaluating our models, enabling us to explore a wide range of material compositions and properties.

Pre-processing Each filtered material was converted into CIF format, ensuring the structural integrity of the original data was preserved. CIF files are widely used in materials science to represent crystal structures and are compatible with various computational tools, facilitating seamless integration into our framework.

In addition to structural data, we enriched our dataset with linguistic descriptions of each material, generated using RoboCrystallographer Ganose & Jain (2019), a tool that automatically produces human-readable summaries of crystallographic information. This step allows for the integration of language-based processing within our framework, leveraging the strengths of large language models. We also extracted key material properties—such as formation energy, total energy, and elemental composition—using the M3GNet Chen & Ong (2022) and PyMatgen Ong et al. (2013) libraries in Python. These properties provide essential inputs for condition-based material design and evaluation within *MatExpert*.

By leveraging this meticulously curated dataset, we ensure that *MatExpert* is evaluated on a robust and diverse set of large-scale materials, facilitating comprehensive assessments of its performance and effectiveness.

5 EXPERIMENTS

5.1 DATASETS AND BASELINES

Material Project: We leverage datasets from the Materials Project database similar to prior studies Xie et al. (2022b); Gruver et al. (2024). The MP-20 dataset (Xie et al., 2022b) for unconditional generation contains 45,231 stable materials, filtered to exclude structures with over 30 atoms per unit cell for computational efficiency. The datasets are exclusively used for the unconditional generation task.

NOMAD: We also collected a large-scale dataset from the NOMAD database, consisting of 2,928,355 materials. The dataset was filtered to exclude structures with inert atoms and more than 30 atoms per unit cell, and it only includes structures computed using VASP in the database. The datasets are exclusively used for the conditional generation task.

To evaluate the effectiveness of MatExpert, we compare its performance against the following state-of-the-art baselines in material generation:

Table 1: MatExpert shows general outperformance compared to baseline methods for unconditional generation on Materials Project based on various metrics like validity checks, coverage, property distribution, and stability. The best results are in **bold**, while the second-best results are underlined.

Method	Validity Check		Coverage		Distribution		Metastable	Stable
	Struc↑	Comp↑	Rec↑	Prec↑	wdist(ρ)↓	wdist(N_{el})↓	M3GNet↑	DFT↑
CDVAE	**1.00**	0.867	0.991	**0.995**	0.68	1.43	28.8%	5.4%
LM-CH	0.848	0.835	0.992	0.978	0.86	0.13	n/a	n/a
LM-AC	0.958	0.889	**0.996**	0.985	0.69	0.09	n/a	n/a
Crystal-LLM with LLaMA-2								
7B ($\tau = 1.0$)	0.918	0.879	0.969	0.960	3.85	0.96	35.1%	6.7%
7B ($\tau = 0.7$)	0.964	0.933	0.911	0.949	3.61	1.06	35.0%	6.2%
70B ($\tau = 1.0$)	0.965	0.863	0.968	0.983	1.72	0.55	35.4%	10.0%
70B ($\tau = 0.7$)	0.996	0.954	0.858	0.989	0.81	0.44	49.8%	10.6%
MatExpert with LLaMA-2								
7B ($\tau = 1.0$)	0.920	0.908	0.984	0.994	0.49	0.11	37.5%	7.8%
7B ($\tau = 0.7$)	0.946	0.943	0.952	0.986	0.51	0.13	36.2%	8.0%
70B ($\tau = 1.0$)	0.968	0.878	0.982	0.986	0.23	0.06	50.2%	11.3%
70B ($\tau = 0.7$)	0.998	0.959	0.969	0.993	0.23	0.07	50.9%	11.8%
MatExpert with LLaMA-3								
8B ($\tau = 1.0$)	0.933	0.910	0.992	**0.995**	0.36	0.07	39.1%	8.1%
8B ($\tau = 0.7$)	0.975	0.959	0.988	0.990	0.38	0.10	39.5%	8.4%
70B ($\tau = 1.0$)	0.970	0.880	0.980	0.988	0.21	0.05	50.5%	11.0%
70B ($\tau = 0.7$)	0.998	**0.961**	0.986	0.991	**0.18**	**0.04**	**51.0%**	**12.0%**

Table 2: Comparison results of conditional generation on NOMAD datasets with MatExpert outperforming baseline methods. The best results are in **bold**.

Method	Validity Check		Coverage		Distribution	
	Struc↑	Comp↑	Rec↑	Prec↑	wdist(ρ)↓	wdist(N_{el})↓
Crystal-LLM with LLaMA-2						
70B ($\tau = 1.0$)	0.983	0.892	0.979	0.984	1.63	0.53
70B ($\tau = 0.7$)	0.997	0.971	0.873	0.988	0.77	0.42
MatExpert with LLaMA-2						
70B ($\tau = 1.0$)	0.991	0.913	0.986	0.992	0.18	**0.08**
70B ($\tau = 0.7$)	0.998	0.981	0.982	0.994	0.21	**0.08**
MatExpert with LLaMA-3						
70B ($\tau = 1.0$)	0.996	0.922	0.991	**0.997**	0.15	**0.08**
70B ($\tau = 0.7$)	**0.999**	**0.986**	**0.989**	0.985	**0.14**	0.09

Crystal-LLM Gruver et al. (2024): A state-of-the-art approach fine-tuning large language models (LLaMA-2 Touvron et al. (2023)) for generating stable inorganic materials. It excels in generating valid crystal structures and serves as a primary baseline due to its pioneering use of LLMs for material generation.

CDVAE Xie et al. (2022b): A Crystal Diffusion Variational Autoencoder tailored for periodic material generation. It combines generative models within a continuous VAE latent space, widely used for generating stable materials and considered a strong benchmark.

LM-CH and LM-AC Flam-Shepherd & Aspuru-Guzik (2023): Transformer-based models for 3D crystal structure generation. LM-CH uses character-level tokenization, while LM-AC uses atom and coordinate-level tokens.

For a fair comparison, MatExpert and baselines are trained on the same datasets for each experiment.

5.2 UNCONDITIONAL GENERATION

In the unconditional generation task, we aim to assess the ability of MatExpert to produce novel and stable material structures without any specific property constraints. This stage serves as a benchmark for evaluating the intrinsic generative capabilities of the model, focusing on the validity, diversity, and stability of the generated materials. For unconditional generation, we randomly select a material from the database during the first stage of MatExpert.

The comparison results are shown in Table 1. As evident from the table, the MatExpert family with LLaMA-3 (Dubey et al., 2024) outperforms all other methods across all metrics except metrics of coverage. Traditional models such as CDVAE, LM-CH, and LM-AC excel in coverage and structural validity. When compared to the state-of-the-art LLM-based model Crystal-LLM, our MatExpert method consistently outperforms Crystal-LLM across all settings, including the same model size and temperature as well as DFT-based stability. Notably, MatExpert achieves remarkable results in distribution metrics, benefiting from the transition from an existing material in the database. While Crystal-LLM may struggle with the hallucinations of LLM, thus generating out-of-distribution materials.

5.3 CONDITIONAL GENERATION

In the conditional generation task, we evaluate MatExpert's ability to generate material structures that meet specific property constraints using the large-scale NOMAD dataset. This task is crucial for practical applications, where researchers often require materials with targeted properties, such as specific band gaps, space groups, and chemical compositions, etc. As shown in Table 2, MatExpert significantly outperforms the baseline Crystal-LLM for all metrics. MatExpert also excels in property distribution, achieving much lower Wasserstein distances, which reflects its ability to generate materials with property distributions closely aligned with the training data. Notably, the stability metric like the energy above the hull is treated as an input property in this task and is not separately evaluated as a performance metric.

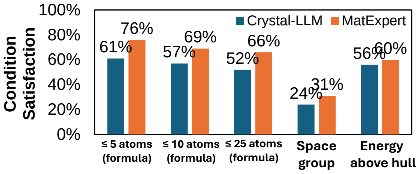

Figure 4: Conditional satisfaction rates of common property constraints. MatExpert consistently outperforms baseline methods.

To rigorously evaluate the effectiveness of MatExpert in satisfying user-defined property constraints, we also conducted additional experiments aimed at quantifying the percentage of generated materials that meet specific property criteria set by users.

We selected a set of common property constraints, including:

- Formula: We parse the composition from the generated CIF. We show the results in three levels by atom numbers: ≤ 5 atoms, ≤ 10 atoms, and ≤ 15 atoms.
- Energy above hull: We use M3GNet Chen & Ong (2022) to estimate the energy above hull. We bin stability as $\hat{E}^{hull} < 0.1$ for metastable and $\hat{E}^{hull} \geq 0.1$ for unstable.
- Space Group Number: We use PyMatgen's SpacegroupAnalyzer with a precision of 0.2 angstroms. Ong et al. (2013)

For each constraint, we generated 10,000 materials using MatExpert and the baselines. We then calculated the percentage of materials that met the specified property criteria. The results of the condition satisfaction experiments are summarized in Figure 4. MatExpert consistently outperformed the baselines across all property constraints, demonstrating its superior capability to generate materials that meet user-defined specifications.

6 ANALYSIS

6.1 ANALYSIS OF DIVERSITY AND NOVELTY

To evaluate the *MatExpert* framework, we use metrics that assess the diversity and novelty of generated materials. Following Xie et al. (2022b), diversity is calculated as the pairwise distance between samples using a featurization of structure and composition. Novelty is determined by comparing the distance to the nearest element of the training set for each sample, with a sample considered novel if this distance exceeds a threshold. We also assess the overall novelty, defined as having either a new structure or composition. To further understand the gaps between MatExpert and baselines, we illustrate the score of each metric normalized to testing samples in Figure 5. As we can see, MatExpert consistently achieves high-level scores in both structure and composition diversity compared to CDVAE and various Crystal-LLM configurations. This indicates MatExpert's superior ability

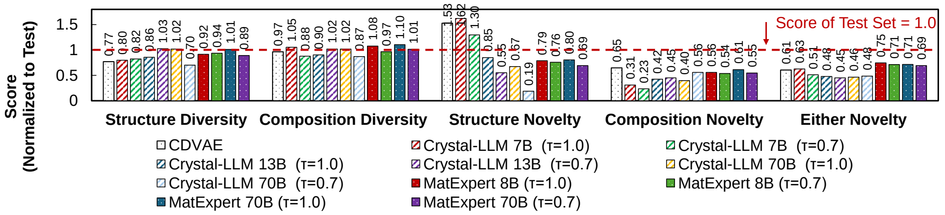

Figure 5: Scores of diversty and novelty normalized to testing samples. MatExpert consistently achieves remarkable scores on all metrics. All socres are calculated on the generated materials passed the validity.

to explore a broad chemical space. In terms of novelty, MatExpert demonstrates a strong capacity to generate structures and compositions not found in existing databases, as evidenced by its high novelty scores. Notably, Crystal-LLM faces challenges in balancing model size and novelty, with larger models exhibiting lower novelty. In contrast, MatExpert consistently maintains high novelty regardless of model size.

6.2 ABLATION STUDIES

To understand the contribution of different components of our framework, we conduct ablation studies by systematically removing or modifying key elements of MatExpert and observing the impact on performance.

Table 3: Choices of encoders in retrieval stage. We use top-1 and top-5 accuracy, along with the average rank of the ground-truth materials as metrics.

Encoder	Accuracy		Avg Rank
	Top-1 (%)	Top-5 (%)	
Bert	59.96	84.51	2.36
T5 (ours)	**71.35**	**93.54**	**1.59**

Impact of Transition (CoT) Stage The transition stage, which involves generating modification pathways using Chain of Thought (CoT) reasoning Wei et al. (2022), plays a crucial role in the overall performance of MatExpert. To evaluate the impact of this component, we conducted experiments where the CoT reasoning was removed entirely. The results in Figure 6 highlight its effectiveness of CoT reasoning.

Impact of Retrieval Stage We assess the impact of the retrieval stage with the contrastive learning framework. By removing the retrieval stage, we observe a noticeable decline in the quality of the retrieved materials (See Figure 6). This confirms that the retrieval stage is crucial for identifying high-quality reference materials, which are essential for effective subsequent modifications.

Choices of Encoders in Retrieval Stage In the retrieval stage, we explored various encoder architectures to determine their impact on the quality of material retrieval (See Table 3). We compared T5-based encoders with BERT Devlin et al. (2019). Our findings indicate that T5-based encoders consistently outperform BERT, providing more accurate embeddings for both property and structure descriptions, making it more effective for capturing the most similar material aligned with the desired properties in the database.

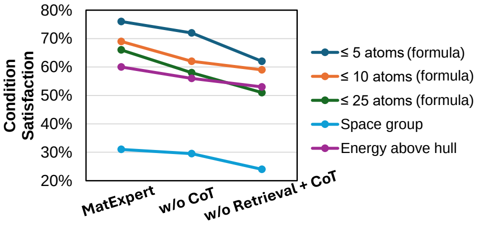

Figure 6: Impact of Transition (CoT) and Retrieval Stages. We sequentially remove the transition (CoT) stage and the retrieval stage to demonstrate changes in condition satisfaction rates.

6.3 CASE STUDY

To showcase the capabilities of MatExpert, we present a comprehensive example of conditional generation under property constraints in Figure 7. This case illustrates the process of generating a predicted material and its adherence to the specified properties.

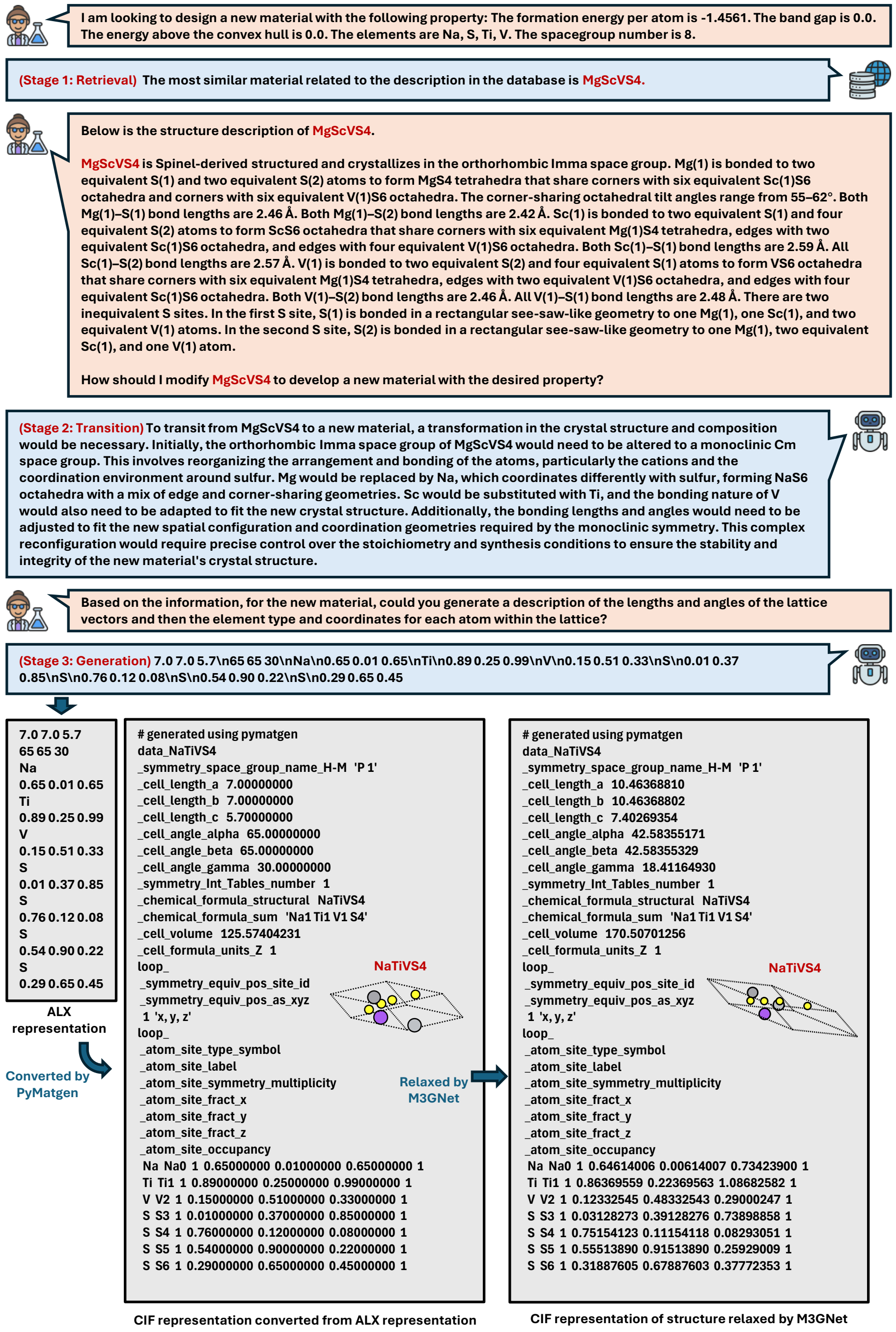

I am looking to design a new material with the following property: The formation energy per atom is -1.4561. The band gap is 0.0. The energy above the convex hull is 0.0. The elements are Na, S, Ti, V. The spacegroup number is 8.

(Stage 1: Retrieval) The most similar material related to the description in the database is MgScVS4.

Below is the structure description of MgScVS4.

MgScVS4 is Spinel-derived structured and crystallizes in the orthorhombic Imma space group. Mg(1) is bonded to two equivalent S(1) and two equivalent S(2) atoms to form MgS4 tetrahedra that share corners with six equivalent Sc(1)S6 octahedra and corners with six equivalent V(1)S6 octahedra. The corner-sharing octahedral tilt angles range from 55–62°. Both Mg(1)–S(1) bond lengths are 2.46 Å. Both Mg(1)–S(2) bond lengths are 2.42 Å. Sc(1) is bonded to two equivalent S(1) and four equivalent S(2) atoms to form ScS6 octahedra that share corners with six equivalent Mg(1)S4 tetrahedra, edges with two equivalent Sc(1)S6 octahedra, and edges with four equivalent V(1)S6 octahedra. Both Sc(1)–S(1) bond lengths are 2.59 Å. All Sc(1)–S(2) bond lengths are 2.57 Å. V(1) is bonded to two equivalent S(2) and four equivalent S(1) atoms to form VS6 octahedra that share corners with six equivalent Mg(1)S4 tetrahedra, edges with two equivalent V(1)S6 octahedra, and edges with four equivalent Sc(1)S6 octahedra. Both V(1)–S(2) bond lengths are 2.46 Å. All V(1)–S(1) bond lengths are 2.48 Å. There are two inequivalent S sites. In the first S site, S(1) is bonded in a rectangular see-saw-like geometry to one Mg(1), one Sc(1), and two equivalent V(1) atoms. In the second S site, S(2) is bonded in a rectangular see-saw-like geometry to one Mg(1), two equivalent Sc(1), and one V(1) atom.

How should I modify MgScVS4 to develop a new material with the desired property?

(Stage 2: Transition) To transit from MgScVS4 to a new material, a transformation in the crystal structure and composition would be necessary. Initially, the orthorhombic Imma space group of MgScVS4 would need to be altered to a monoclinic Cm space group. This involves reorganizing the arrangement and bonding of the atoms, particularly the cations and the coordination environment around sulfur. Mg would be replaced by Na, which coordinates differently with sulfur, forming NaS6 octahedra with a mix of edge and corner-sharing geometries. Sc would be substituted with Ti, and the bonding nature of V would also need to be adapted to fit the new crystal structure. Additionally, the bonding lengths and angles would need to be adjusted to fit the new spatial configuration and coordination geometries required by the monoclinic symmetry. This complex reconfiguration would require precise control over the stoichiometry and synthesis conditions to ensure the stability and integrity of the new material's crystal structure.

Based on the information, for the new material, could you generate a description of the lengths and angles of the lattice vectors and then the element type and coordinates for each atom within the lattice?

(Stage 3: Generation) 7.0 7.0 5.7\n65 65 30\nNa\n0.65 0.01 0.65\nTi\n0.89 0.25 0.99\nV\n0.15 0.51 0.33\nS\n0.01 0.37 0.85\nS\n0.76 0.12 0.08\nS\n0.54 0.90 0.22\nS\n0.29 0.65 0.45

```
7.0 7.0 5.7
65 65 30
Na
0.65 0.01 0.65
Ti
0.89 0.25 0.99
V
0.15 0.51 0.33
S
0.01 0.37 0.85
S
0.76 0.12 0.08
S
0.54 0.90 0.22
S
0.29 0.65 0.45
```

ALX representation

```
# generated using pymatgen
data_NaTiVS4
_symmetry_space_group_name_H-M  'P 1'
_cell_length_a  7.00000000
_cell_length_b  7.00000000
_cell_length_c  5.70000000
_cell_angle_alpha  65.00000000
_cell_angle_beta  65.00000000
_cell_angle_gamma  30.00000000
_symmetry_Int_Tables_number  1
_chemical_formula_structural  NaTiVS4
_chemical_formula_sum  'Na1 Ti1 V1 S4'
_cell_volume  125.57404231
_cell_formula_units_Z  1
loop_
 _symmetry_equiv_pos_site_id
 _symmetry_equiv_pos_as_xyz
  1  'x, y, z'
loop_
 _atom_site_type_symbol
 _atom_site_label
 _atom_site_symmetry_multiplicity
 _atom_site_fract_x
 _atom_site_fract_y
 _atom_site_fract_z
 _atom_site_occupancy
  Na  Na0  1  0.65000000  0.01000000  0.65000000  1
  Ti  Ti1  1  0.89000000  0.25000000  0.99000000  1
  V  V2  1  0.15000000  0.51000000  0.33000000  1
  S  S3  1  0.01000000  0.37000000  0.85000000  1
  S  S4  1  0.76000000  0.12000000  0.08000000  1
  S  S5  1  0.54000000  0.90000000  0.22000000  1
  S  S6  1  0.29000000  0.65000000  0.45000000  1
```

CIF representation converted from ALX representation

```
# generated using pymatgen
data_NaTiVS4
_symmetry_space_group_name_H-M  'P 1'
_cell_length_a  10.46368810
_cell_length_b  10.46368802
_cell_length_c  7.40269354
_cell_angle_alpha  42.58355171
_cell_angle_beta  42.58355329
_cell_angle_gamma  18.41164930
_symmetry_Int_Tables_number  1
_chemical_formula_structural  NaTiVS4
_chemical_formula_sum  'Na1 Ti1 V1 S4'
_cell_volume  170.50701256
_cell_formula_units_Z  1
loop_
 _symmetry_equiv_pos_site_id
 _symmetry_equiv_pos_as_xyz
  1  'x, y, z'
loop_
 _atom_site_type_symbol
 _atom_site_label
 _atom_site_symmetry_multiplicity
 _atom_site_fract_x
 _atom_site_fract_y
 _atom_site_fract_z
 _atom_site_occupancy
  Na  Na0  1  0.64614006  0.00614007  0.73423900  1
  Ti  Ti1  1  0.86369559  0.22369563  1.08682582  1
  V  V2  1  0.12332545  0.48332543  0.29000247  1
  S  S3  1  0.03128273  0.39128276  0.73898858  1
  S  S4  1  0.75154123  0.11154118  0.08293051  1
  S  S5  1  0.55513890  0.91513890  0.25929009  1
  S  S6  1  0.31887605  0.67887603  0.37772353  1
```

CIF representation of structure relaxed by M3GNet

Figure 7: A comprehensive example of MatExpert for conditional generation: Enter the desired properties, and MatExpert will generate the CIF representation of the material.

7 CONCLUSION

In this work, we introduced MatExpert, a novel framework leveraging LLMs and contrastive learning for the material discovery process. By emulating the workflow of a human materials science expert, MatExpert integrates retrieval, transition, and generation stages to design new materials. Our experiments show that MatExpert significantly outperforms state-of-the-art methods in material generation tasks, thereby exhibiting its potential to become a scalable tool for accelerating material discovery with higher-quality crystal generation.

REFERENCES

Nawaf Alampara, Santiago Miret, and Kevin Maik Jablonka. Mattext: Do language models need more than text & scale for materials modeling? In *AI for Accelerated Materials Design-Vienna 2024*, 2024.

Luis M Antunes, Keith T Butler, and Ricardo Grau-Crespo. Crystal structure generation with autoregressive large language modeling. *arXiv preprint arXiv:2307.04340*, 2023.

Chi Chen and Shyue Ping Ong. A universal graph deep learning interatomic potential for the periodic table. *Nature Computational Science*, 2(11):718–728, 2022.

Ting Chen, Simon Kornblith, Mohammad Norouzi, and Geoffrey E. Hinton. A simple framework for contrastive learning of visual representations. In *ICML*, volume 119 of *Proceedings of Machine Learning Research*, pp. 1597–1607. PMLR, 2020.

Callum J Court, Batuhan Yildirim, Apoorv Jain, and Jacqueline M Cole. 3-d inorganic crystal structure generation and property prediction via representation learning. *Journal of Chemical Information and Modeling*, 60(10):4518–4535, 2020.

Tri Dao, Dan Fu, Stefano Ermon, Atri Rudra, and Christopher Ré. Flashattention: Fast and memory-efficient exact attention with io-awareness. *Advances in Neural Information Processing Systems*, 35:16344–16359, 2022.

Grégoire Delétang, Anian Ruoss, Paul-Ambroise Duquenne, Elliot Catt, Tim Genewein, Christopher Mattern, Jordi Grau-Moya, Li Kevin Wenliang, Matthew Aitchison, Laurent Orseau, et al. Language modeling is compression. *arXiv preprint arXiv:2309.10668*, 2023.

Jacob Devlin, Ming-Wei Chang, Kenton Lee, and Kristina Toutanova. Bert: Pre-training of deep bidirectional transformers for language understanding. In *Proceedings of the 2019 Conference of the North American Chapter of the Association for Computational Linguistics: Human Language Technologies, Volume 1 (Long and Short Papers)*, pp. 4171–4186, 2019.

Abhimanyu Dubey, Abhinav Jauhri, Abhinav Pandey, Abhishek Kadian, Ahmad Al-Dahle, Aiesha Letman, Akhil Mathur, Alan Schelten, Amy Yang, Angela Fan, et al. The llama 3 herd of models. *arXiv preprint arXiv:2407.21783*, 2024.

Alexandre Duval, Simon V Mathis, Chaitanya K Joshi, Victor Schmidt, Santiago Miret, Fragkiskos D Malliaros, Taco Cohen, Pietro Lio, Yoshua Bengio, and Michael Bronstein. A hitchhiker's guide to geometric gnns for 3d atomic systems. *arXiv preprint arXiv:2312.07511*, 2023.

Daniel Flam-Shepherd and Alán Aspuru-Guzik. Language models can generate molecules, materials, and protein binding sites directly in three dimensions as xyz, cif, and pdb files. *arXiv preprint arXiv:2305.05708*, 2023.

Alex M Ganose and Anubhav Jain. Robocrystallographer: automated crystal structure text descriptions and analysis. *MRS Communications*, 9(3):874–881, 2019.

Prashant Govindarajan, Santiago Miret, Jarrid Rector-Brooks, Mariano Phielipp, Janarthanan Rajendran, and Sarath Chandar. Learning conditional policies for crystal design using offline reinforcement learning. *Digital Discovery*, 3(4):769–785, 2024.

Nate Gruver, Anuroop Sriram, Andrea Madotto, Andrew Gordon Wilson, C. Lawrence Zitnick, and Zachary Ward Ulissi. Fine-tuned language models generate stable inorganic materials as text. In *AI for Accelerated Materials Design - NeurIPS 2023 Workshop*, 2023. URL `https://openreview.net/forum?id=0r5DE2ZSwJ`.

Nate Gruver, Anuroop Sriram, Andrea Madotto, Andrew Gordon Wilson, C. Lawrence Zitnick, and Zachary W. Ulissi. Fine-tuned language models generate stable inorganic materials as text. In *ICLR*. OpenReview.net, 2024.

Kausik Hira, Mohd Zaki, Dhruvil Sheth, NM Anoop Krishnan, et al. Reconstructing the materials tetrahedron: challenges in materials information extraction. *Digital Discovery*, 3(5):1021–1037, 2024.

Edward J Hu, Yelong Shen, Phillip Wallis, Zeyuan Allen-Zhu, Yuanzhi Li, Shean Wang, Lu Wang, and Weizhu Chen. LoRA: Low-rank adaptation of large language models. In *International Conference on Learning Representations*, 2022. URL `https://openreview.net/forum?id=nZeVKeeFYf9`.

Kevin Maik Jablonka, Philippe Schwaller, Andres Ortega-Guerrero, and Berend Smit. Leveraging large language models for predictive chemistry. *Nature Machine Intelligence*, 6(2):161–169, 2024.

Anubhav Jain, Shyue Ping Ong, Geoffroy Hautier, Wei Chen, William Davidson Richards, Stephen Dacek, Shreyas Cholia, Dan Gunter, David Skinner, Gerbrand Ceder, et al. Commentary: The materials project: A materials genome approach to accelerating materials innovation. *APL materials*, 1(1), 2013.

Rui Jiao, Wenbing Huang, Peijia Lin, Jiaqi Han, Pin Chen, Yutong Lu, and Yang Liu. Crystal structure prediction by joint equivariant diffusion. *Advances in Neural Information Processing Systems*, 36, 2024.

Georg Kresse and Jürgen Hafner. Ab initio molecular dynamics for liquid metals. *Physical review B*, 47(1):558, 1993.

Haokun Liu, Derek Tam, Mohammed Muqeeth, Jay Mohta, Tenghao Huang, Mohit Bansal, and Colin A Raffel. Few-shot parameter-efficient fine-tuning is better and cheaper than in-context learning. *Advances in Neural Information Processing Systems*, 35:1950–1965, 2022.

Benjamin Kurt Miller, Ricky T. Q. Chen, Anuroop Sriram, and Brandon M Wood. FlowMM: Generating materials with riemannian flow matching. In *Forty-first International Conference on Machine Learning*, 2024. URL `https://openreview.net/forum?id=W4pB7VbzZI`.

Santiago Miret and NM Krishnan. Are llms ready for real-world materials discovery? *arXiv preprint arXiv:2402.05200*, 2024.

Santiago Miret, NM Anoop Krishnan, Benjamin Sanchez-Lengeling, Marta Skreta, Vineeth Venugopal, and Jennifer N Wei. Perspective on ai for accelerated materials design at the ai4mat-2023 workshop at neurips 2023. *Digital Discovery*, 2024.

Adrian Mirza, Nawaf Alampara, Sreekanth Kunchapu, Benedict Emoekabu, Aswanth Krishnan, Mara Wilhelmi, Macjonathan Okereke, Juliane Eberhardt, Amir Mohammad Elahi, Maximilian Greiner, et al. Are large language models superhuman chemists? *arXiv preprint arXiv:2404.01475*, 2024.

Vaibhav Mishra, Somaditya Singh, Mohd Zaki, Hargun Singh Grover, Santiago Miret, Mausam ., and N M Anoop Krishnan. LLamat: Large language models for materials science. In *AI for Accelerated Materials Design - Vienna 2024*, 2024. URL `https://openreview.net/forum?id=ZUkmRy6SqS`.

Shyue Ping Ong, William Davidson Richards, Anubhav Jain, Geoffroy Hautier, Michael Kocher, Shreyas Cholia, Dan Gunter, Vincent L Chevrier, Kristin A Persson, and Gerbrand Ceder. Python materials genomics (pymatgen): A robust, open-source python library for materials analysis. *Computational Materials Science*, 68:314–319, 2013.

OpenAI. GPT-4 technical report. *CoRR*, abs/2303.08774, 2023.

Alec Radford, Jong Wook Kim, Chris Hallacy, Aditya Ramesh, Gabriel Goh, Sandhini Agarwal, Girish Sastry, Amanda Askell, Pamela Mishkin, Jack Clark, et al. Learning transferable visual models from natural language supervision. In *International conference on machine learning*, pp. 8748–8763. PMLR, 2021.

Colin Raffel, Noam Shazeer, Adam Roberts, Katherine Lee, Sharan Narang, Michael Matena, Yanqi Zhou, Wei Li, and Peter J Liu. Exploring the limits of transfer learning with a unified text-to-text transformer. *Journal of machine learning research*, 21(140):1–67, 2020.

Mayk Caldas Ramos, Christopher J Collison, and Andrew D White. A review of large language models and autonomous agents in chemistry. *arXiv preprint arXiv:2407.01603*, 2024.

Janosh Riebesell, Rhys EA Goodall, Anubhav Jain, Philipp Benner, Kristin A Persson, and Alpha A Lee. Matbench discovery–an evaluation framework for machine learning crystal stability prediction. *arXiv preprint arXiv:2308.14920*, 2023.

Markus Scheidgen, Lauri Himanen, Alvin Noe Ladines, David Sikter, Mohammad Nakhaee, Ádám Fekete, Theodore Chang, Amir Golparvar, José A Márquez, Sandor Brockhauser, Sebastian BrÃ¼ckner, Luca M. Ghiringhelli, Felix Dietrich, Daniel Lehmberg, Thea Denell, Andrea Albino, Hampus Naesstroem, Sherjeel Shabih, Florian Dobener, Markus KÃ¼hbach, Rubel Mozumder, Joseph F. Rudzinski, Nathan Daelman, José M. Pizarro, Martin Kuban, Cuauhtemoc Salazar, Pavel Ondracka, Hans-Joachim Bungartz, and Claudia Draxl. Nomad: A distributed web-based platform for managing materials science research data. *Journal of Open Source Software*, 8(90):5388, 2023. doi: 10.21105/joss.05388. URL `https://doi.org/10.21105/joss.05388`.

Mara Schilling-Wilhelmi, Martiño Ríos-García, Sherjeel Shabih, María Victoria Gil, Santiago Miret, Christoph T Koch, José A Márquez, and Kevin Maik Jablonka. From text to insight: Large language models for materials science data extraction. *arXiv preprint arXiv:2407.16867*, 2024.

Amanpreet Singh, Ronghang Hu, Vedanuj Goswami, Guillaume Couairon, Wojciech Galuba, Marcus Rohrbach, and Douwe Kiela. Flava: A foundational language and vision alignment model. In *Proceedings of the IEEE/CVF Conference on Computer Vision and Pattern Recognition*, pp. 15638–15650, 2022.

Yu Song, Santiago Miret, and Bang Liu. Matsci-nlp: Evaluating scientific language models on materials science language tasks using text-to-schema modeling. In *Proceedings of the 61st Annual Meeting of the Association for Computational Linguistics (Volume 1: Long Papers)*, pp. 3621–3639, 2023a.

Yu Song, Santiago Miret, Huan Zhang, and Bang Liu. Honeybee: Progressive instruction finetuning of large language models for materials science. In *Findings of the Association for Computational Linguistics: EMNLP 2023*, pp. 5724–5739, 2023b.

Hugo Touvron, Louis Martin, Kevin Stone, Peter Albert, Amjad Almahairi, Yasmine Babaei, Nikolay Bashlykov, Soumya Batra, Prajjwal Bhargava, Shruti Bhosale, Dan Bikel, Lukas Blecher, Cristian Canton-Ferrer, Moya Chen, Guillem Cucurull, David Esiobu, Jude Fernandes, Jeremy Fu, Wenyin Fu, Brian Fuller, Cynthia Gao, Vedanuj Goswami, Naman Goyal, Anthony Hartshorn, Saghar Hosseini, Rui Hou, Hakan Inan, Marcin Kardas, Viktor Kerkez, Madian Khabsa, Isabel Kloumann, Artem Korenev, Punit Singh Koura, Marie-Anne Lachaux, Thibaut Lavril, Jenya Lee, Diana Liskovich, Yinghai Lu, Yuning Mao, Xavier Martinet, Todor Mihaylov, Pushkar Mishra, Igor Molybog, Yixin Nie, Andrew Poulton, Jeremy Reizenstein, Rashi Rungta, Kalyan Saladi, Alan Schelten, Ruan Silva, Eric Michael Smith, Ranjan Subramanian, Xiaoqing Ellen Tan, Binh Tang, Ross Taylor, Adina Williams, Jian Xiang Kuan, Puxin Xu, Zheng Yan, Iliyan Zarov, Yuchen Zhang, Angela Fan, Melanie Kambadur, Sharan Narang, Aurélien Rodriguez, Robert Stojnic, Sergey Edunov, and Thomas Scialom. Llama 2: Open foundation and fine-tuned chat models. *CoRR*, abs/2307.09288, 2023.

Jason Wei, Xuezhi Wang, Dale Schuurmans, Maarten Bosma, Fei Xia, Ed Chi, Quoc V Le, Denny Zhou, et al. Chain-of-thought prompting elicits reasoning in large language models. *Advances in neural information processing systems*, 35:24824–24837, 2022.

T Wolf. Huggingface's transformers: State-of-the-art natural language processing. *arXiv preprint arXiv:1910.03771*, 2019.

Tian Xie, Xiang Fu, Octavian Ganea, Regina Barzilay, and Tommi Jaakkola. Crystal diffusion variational autoencoder for periodic material generation. *Bulletin of the American Physical Society*, 67, 2022a.

Tian Xie, Xiang Fu, Octavian-Eugen Ganea, Regina Barzilay, and Tommi S. Jaakkola. Crystal diffusion variational autoencoder for periodic material generation. In *ICLR*. OpenReview.net, 2022b.

Tong Xie, Yuwei Wan, Wei Huang, Zhenyu Yin, Yixuan Liu, Shaozhou Wang, Qingyuan Linghu, Chunyu Kit, Clara Grazian, Wenjie Zhang, et al. Darwin series: Domain specific large language models for natural science. *arXiv preprint arXiv:2308.13565*, 2023.

Minghao Xu, Xinyu Yuan, Santiago Miret, and Jian Tang. Protst: Multi-modality learning of protein sequences and biomedical texts. In *International Conference on Machine Learning*, pp. 38749–38767. PMLR, 2023.

Sherry Yang, KwangHwan Cho, Amil Merchant, Pieter Abbeel, Dale Schuurmans, Igor Mordatch, and Ekin Dogus Cubuk. Scalable diffusion for materials generation. In *The Twelfth International Conference on Learning Representations*, 2024. URL `https://openreview.net/forum?id=wm4WlHoXpC`.

Claudio Zeni, Robert Pinsler, Daniel Zügner, Andrew Fowler, Matthew Horton, Xiang Fu, Sasha Shysheya, Jonathan Crabbé, Lixin Sun, Jake Smith, et al. Mattergen: a generative model for inorganic materials design. *arXiv preprint arXiv:2312.03687*, 2023.

Huan Zhang, Yu Song, Ziyu Hou, Santiago Miret, and Bang Liu. Honeycomb: A flexible llm-based agent system for materials science. *arXiv preprint arXiv:2409.00135*, 2024.

Yaowei Zheng, Richong Zhang, Junhao Zhang, Yanhan Ye, and Zheyan Luo. Llamafactory: Unified efficient fine-tuning of 100+ language models. *arXiv preprint arXiv:2403.13372*, 2024.

A REPRODUCIBLITY

A.1 ENVIRONMENT

The experiments were conducted on machines with the following specifications.

Machine 1 for MatExpert with Llama-2 8B and Llama-3 8B:

- **Hardware:** NVIDIA A5000 GPU (24 GB on-board memory) GPU x 4, AMD Ryzen Threadripper PRO 3975WX CPU, 256 GB RAM
- **Software:** Ubuntu 22.04, Python 3.11, PyTorch 2.3.1+cu121, CUDA 12.4

Machine 2 for MatExpert with Llama-2 70B and Llama-3 70B:

- **Hardware:** NVIDIA L40S GPU (48 GB on-board memory) x 4, INTEL(R) XEON(R) GOLD 6526Y x 2, 512 GB RAM
- **Software:** Ubuntu 22.04, Python 3.11, PyTorch 2.3.1+cu121, CUDA 12.4

The list of environment requirements for the Python library will be made publicly available alongside the release of the open-source code of MatExpert.

A.2 IMPLEMENTATION DETAILS

Table 4: Hyperparameters for training T5-based encoders in the retrieval stage.

Hyperparameter	**Value**	**Description**
Model Architecture	t5-base	Pretrained model to use as the base encoder.
Learning Rate	1e-4	Learning rate for the optimizer.
Number of epochs	100	Number of epochs to train for.
Temperature	0.1	Temperature parameter for the NT-Xent loss.
Batch Size	32	Batch size for training.
Gradient Accumulation Steps	8	Number of batches for gradient accumulation.

Table 5: Hyperparameters for finetuning Llama family in the transition and generation stage.

Hyperparameter	**Llama-3 8B**	**Llama-3 70B**
Model Architecture	Meta-Llama-3-8B-Instruct	Meta-Llama-3-70B-Instruct
Learning Rate	$1e^{-4}$	$1e^{-4}$
Batch Size	4	4
Batch Size per Device	1	1
Number of Epochs	70	10
Optimizer	AdamW	AdamW
Sequence Length	2048	1024
LoRA Rank	8	8
LoRA Alpha	16	16
LoRA Dropout	0.1	0.1
Warmup Ratio	0.1	0.1
Gradient Accumulation Steps	8	8

The proposed MatExprt framework consists of two training stages: 1) Training T5-based encoders of the contrastive learning framework in the stage Retrieval. 2) Finetuning the Llama-2/Llama-3 based LLMs in the stage Transition and stage Generation.

Training T5-based encoders In the retrieval stage, two T5-based encoders are employed. The model uses the ”t5-base” architecture in Huggingface Wolf (2019) as its foundational structure. The training process is governed by a learning rate of 0.0001. It undergoes training for 100 epochs with early stopping. A temperature parameter of 0.1 is utilized, which affects the NT-Xent loss function, a common choice for contrastive learning. The batch size is set to 32 and gradient accumulation occurs over 8 steps, effectively simulating a larger batch size and allowing for more stable updates.

Finetuning Llama family In the transition and generation stages, the Llama family of models is finetuned. Two variants are used: Llama-3 8B and Llama-3 70B, both with specific architectures designed for instruction-based tasks named “Meta-Llama-3-8B-Instruct” and “Meta-Llama-3-70B-Instruct” in Huggingface Wolf (2019). The learning rate is set to 0.0001. Each device processes a batch size of 1, with an overall batch size of 4. The 8B model is trained for 70 epochs, while the 70B model undergoes 10 epochs, reflecting differences in their complexity and training needs. The AdamW optimizer is employed for parameter updates. Sequence lengths differ, with the 8B model handling sequences of 2048 tokens, and the 70B model processing 1024 tokens limited by the on-board memory of GPUs. LoRA settings include a rank of 8, an alpha of 16, and a dropout rate of 0.1, facilitating efficient adaptation. A warmup ratio of 0.1 helps stabilize initial training and gradient accumulation is set to 8 steps for both models, ensuring robust learning.

A.3 EFFICIENCY

We utilize the open-source LLM training framework named LLaMA-Factory Zheng et al. (2024) to finetune the LLMs. With the advantages of LoRA Hu et al. (2022) and FlashAttention Dao et al. (2022) mechanism, it takes around 30 and 120 hours to fine-tune Llama-3 8B and Llama-3 70B in MatExpert, respectively.

The generation speed of MatExpert on our machines is as follows:

- MatExpert with Llama-3 8B: ∼40 minutes per 10,000 samples.
- MatExpert with Llama-3 70B: ∼5 hours per 10,000 samples.

B DATASETS DETAILS

Two datasets are included in our experiments: Material Project and NOMAD for unconditional generation and conditional generation, respectively.

Material Project This dataset also named as MP-20 consisting of 45,231 materials is publicly available and was first proposed in Ong et al. (2013). We follow the data-split setting proposed in Gruver et al. (2023) and Xie et al. (2022a).

NOMAD This large-scale dataset consisting of 2,886,120 materials is collected by ourselves and will be publicly available. We collect the datasets via NOMAD API as the following script:

```
url = ’http://nomad-lab.eu/prod/v1/api/v1/entries/archive/query’
excluded_elements = [
    "He", "Ne", "Ar", "Kr", "Xe", "Rn", "U", "Th", "Rn", "Tc",
    "Po", "Pu", "Pa",
]
query = {
    "results.method.simulation.program_name:any": [
        "VASP"
    ],
    "quantities:all": [
        "results.properties.structures",
        "results.properties.structures.structure_original",
        "results.properties.structures.structure_conventional",
        "results.properties.structures.structure_primitive"
    ]
}
required = {
    "results": {
        "material": {
            "chemical_formula_reduced": "*"
        },
        "properties": {
            "structures": "*"
        }
    }
}
```

We filter out the materials with elements in `excluded_elements` and only include the materials with structures computing by VASP Kresse & Hafner (1993).

Then we further convert the structure in JSON to CIF files via the following script:

```
def convert_to_cif(structure_json, lattice='vectors'):
    lattice_vectors = structure_json["lattice_vectors"]
    lattice_parameters = structure_json["lattice_parameters"]
    a = lattice_parameters["a"]
    b = lattice_parameters["b"]
    c = lattice_parameters["c"]
    alpha = lattice_parameters["alpha"] * 180 / np.pi
    beta = lattice_parameters["beta"] * 180 / np.pi
    gamma = lattice_parameters["gamma"] * 180 / np.pi

    if lattice == 'vectors':
        lattice = Lattice(lattice_vectors)
    elif lattice == 'parameters':
        lattice = Lattice.from_parameters(a, b, c, alpha, beta, gamma)

    positions = structure_json["cartesian_site_positions"]
    species = structure_json["species_at_sites"]

    structure = Structure(lattice, species, positions, coords_are_cartesian=True)
    structure.scale_lattice(1000)

    return structure.to(fmt="cif")
```

We randomly select 10,000 samples and another 10,000 samples as the validation and testing set, respectively. The remaining samples are all included in the training set.

C EVALUATION METRICS

C.1 VALIDITY

Validity is evaluated based on the structural and compositional integrity of the generated materials. Following Xie et al. (2022a), a structure is considered valid if the shortest distance between any pair of atoms is greater than 0.5 Å, ensuring atomic stability. Furthermore, the overall charge of the material must be neutral to satisfy chemical feasibility. These criteria ensure that the generated materials conform to realistic physical and chemical constraints.

C.2 COVERAGE

Following the methods outlined in Xie et al. (2022a) and Gruver et al. (2023), we measure coverage using two metrics: COV-R (Recall) and COV-P (Precision). These metrics quantify how well the generated materials resemble the ground truth materials in the test set. COV-R (Recall) measures the percentage of ground truth materials accurately represented by the generated set, while COV-P (Precision) evaluates the quality of the generated materials in replicating the true material diversity. These metrics ensure that the generated materials not only capture the diversity of the test set but also maintain high-quality representations. Both validity and coverage are computed over 10,000 materials randomly sampled from the generated set.

C.3 DISTRIBUTION

The distribution of properties is compared between the generated materials and the test set using the Wasserstein distance. The key properties evaluated are density (ρ, measured in g/cm^3) and the number of unique elements (N_{el}). The property distribution is computed over 1,000 valid materials, randomly sampled from those that pass the validity test. This method ensures that the generated materials exhibit realistic physical properties comparable to those in the test set.

C.4 DIVERSITY

Diversity is assessed by calculating the pairwise distances between samples, based on structural and compositional features as described by Court et al. (2020). This metric quantifies how distinct each generated sample is relative to others in the dataset, offering insights into the variety of structures and compositions. Diversity is specifically measured on samples deemed metastable by M3GNet, as these are more likely to contribute meaningful variation. All diversity values are normalized against corresponding metrics from the test set, providing a clear comparison of the underlying data distributions.

C.5 NOVELTY

Novelty is calculated by comparing each generated sample to its nearest neighbor in the training set. A sample is considered novel if its nearest neighbor exceeds a predefined threshold distance. Specifically, we use a structural distance cutoff of 0.1 and a compositional distance cutoff of 2. Novelty is assessed both in terms of structure and composition, with overall crystal novelty determined by the presence of a new structure or composition. These metrics provide insights into the uniqueness of the generated samples, particularly those identified as metastable. Novelty values are normalized by corresponding values for the test set to effectively convey the characteristics of the data distribution.

C.6 STABILITY

We assess the stability of materials using a combination of machine learning potentials and density functional theory (DFT) to ensure a consistent evaluation framework. Specifically, we employ the M3GNet model Chen & Ong (2022), trained on total energy data from VASP calculations within the Materials Project dataset. This aligns the results with established correction schemes and absolute energy values. For consistency with Materials Project settings and prior works Xie et al. (2022a); Gruver et al. (2023), including the PBE functional and DFT/DFT+U, we perform a single relaxation for each candidate structure using the default MPRelaSet parameters.

To determine the percentage of metastable compounds, we first filter out samples that fail basic structural and compositional validity checks. The remaining samples are then relaxed using M3GNet to obtain final relaxation energies. The stability calculation includes the validity rate from initial filtering and the rate of compounds with relaxed hull energy $\hat{E}_{\text{hull}} < 0.1$. For stable materials, those identified as metastable by M3GNet undergo further DFT relaxation, and the percentage with $\hat{E}_{\text{hull}} < 0.0$ is reported. This comprehensive approach integrates both machine learning and traditional DFT methods for a robust stability evaluation.

D CASES OF UNCONDITIONAL GENERATION

Please see Figure 8.

E CASES OF CONDITIONAL GENERATION

Please see Figure 9.

F NUMERICAL RESULTS OF ABLATION STUDY (FIGURE 6)

Please see Table 6.

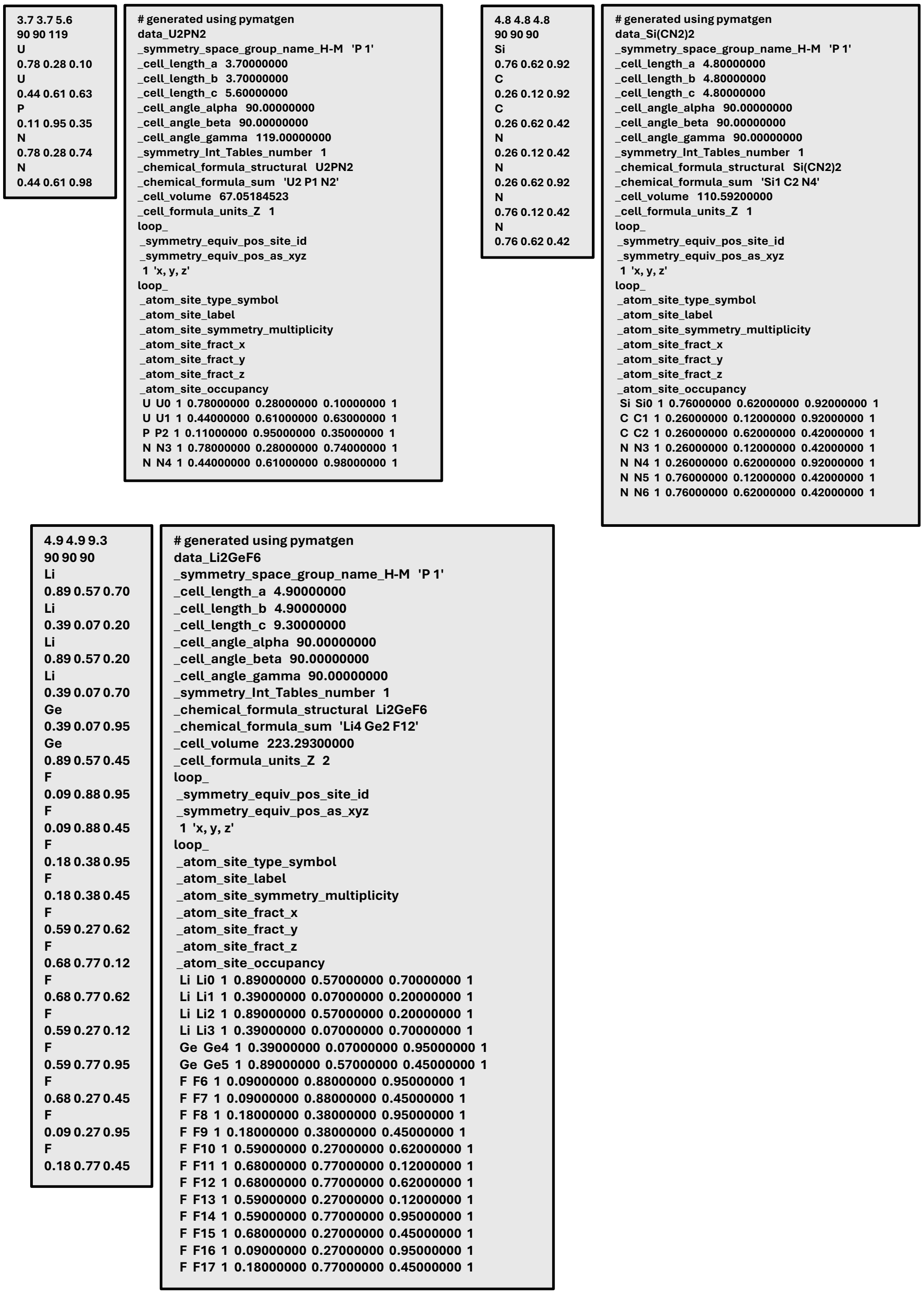

```
3.7 3.7 5.6
90 90 119
U
0.78 0.28 0.10
U
0.44 0.61 0.63
P
0.11 0.95 0.35
N
0.78 0.28 0.74
N
0.44 0.61 0.98
```

```
# generated using pymatgen
data_U2PN2
_symmetry_space_group_name_H-M   'P 1'
_cell_length_a   3.70000000
_cell_length_b   3.70000000
_cell_length_c   5.60000000
_cell_angle_alpha   90.00000000
_cell_angle_beta   90.00000000
_cell_angle_gamma   119.00000000
_symmetry_Int_Tables_number   1
_chemical_formula_structural   U2PN2
_chemical_formula_sum   'U2 P1 N2'
_cell_volume   67.05184523
_cell_formula_units_Z   1
loop_
 _symmetry_equiv_pos_site_id
 _symmetry_equiv_pos_as_xyz
  1  'x, y, z'
loop_
 _atom_site_type_symbol
 _atom_site_label
 _atom_site_symmetry_multiplicity
 _atom_site_fract_x
 _atom_site_fract_y
 _atom_site_fract_z
 _atom_site_occupancy
  U  U0  1  0.78000000  0.28000000  0.10000000  1
  U  U1  1  0.44000000  0.61000000  0.63000000  1
  P  P2  1  0.11000000  0.95000000  0.35000000  1
  N  N3  1  0.78000000  0.28000000  0.74000000  1
  N  N4  1  0.44000000  0.61000000  0.98000000  1
```

```
4.8 4.8 4.8
90 90 90
Si
0.76 0.62 0.92
C
0.26 0.12 0.92
C
0.26 0.62 0.42
N
0.26 0.12 0.42
N
0.26 0.62 0.92
N
0.76 0.12 0.42
N
0.76 0.62 0.42
```

```
# generated using pymatgen
data_Si(CN2)2
_symmetry_space_group_name_H-M   'P 1'
_cell_length_a   4.80000000
_cell_length_b   4.80000000
_cell_length_c   4.80000000
_cell_angle_alpha   90.00000000
_cell_angle_beta   90.00000000
_cell_angle_gamma   90.00000000
_symmetry_Int_Tables_number   1
_chemical_formula_structural   Si(CN2)2
_chemical_formula_sum   'Si1 C2 N4'
_cell_volume   110.59200000
_cell_formula_units_Z   1
loop_
 _symmetry_equiv_pos_site_id
 _symmetry_equiv_pos_as_xyz
  1  'x, y, z'
loop_
 _atom_site_type_symbol
 _atom_site_label
 _atom_site_symmetry_multiplicity
 _atom_site_fract_x
 _atom_site_fract_y
 _atom_site_fract_z
 _atom_site_occupancy
  Si  Si0  1  0.76000000  0.62000000  0.92000000  1
  C  C1  1  0.26000000  0.12000000  0.92000000  1
  C  C2  1  0.26000000  0.62000000  0.42000000  1
  N  N3  1  0.26000000  0.12000000  0.42000000  1
  N  N4  1  0.26000000  0.62000000  0.92000000  1
  N  N5  1  0.76000000  0.12000000  0.42000000  1
  N  N6  1  0.76000000  0.62000000  0.42000000  1
```

```
4.9 4.9 9.3
90 90 90
Li
0.89 0.57 0.70
Li
0.39 0.07 0.20
Li
0.89 0.57 0.20
Li
0.39 0.07 0.70
Ge
0.39 0.07 0.95
Ge
0.89 0.57 0.45
F
0.09 0.88 0.95
F
0.09 0.88 0.45
F
0.18 0.38 0.95
F
0.18 0.38 0.45
F
0.59 0.27 0.62
F
0.68 0.77 0.12
F
0.68 0.77 0.62
F
0.59 0.27 0.12
F
0.59 0.77 0.95
F
0.68 0.27 0.45
F
0.09 0.27 0.95
F
0.18 0.77 0.45
```

```
# generated using pymatgen
data_Li2GeF6
_symmetry_space_group_name_H-M   'P 1'
_cell_length_a   4.90000000
_cell_length_b   4.90000000
_cell_length_c   9.30000000
_cell_angle_alpha   90.00000000
_cell_angle_beta   90.00000000
_cell_angle_gamma   90.00000000
_symmetry_Int_Tables_number   1
_chemical_formula_structural   Li2GeF6
_chemical_formula_sum   'Li4 Ge2 F12'
_cell_volume   223.29300000
_cell_formula_units_Z   2
loop_
 _symmetry_equiv_pos_site_id
 _symmetry_equiv_pos_as_xyz
  1  'x, y, z'
loop_
 _atom_site_type_symbol
 _atom_site_label
 _atom_site_symmetry_multiplicity
 _atom_site_fract_x
 _atom_site_fract_y
 _atom_site_fract_z
 _atom_site_occupancy
  Li  Li0  1  0.89000000  0.57000000  0.70000000  1
  Li  Li1  1  0.39000000  0.07000000  0.20000000  1
  Li  Li2  1  0.89000000  0.57000000  0.20000000  1
  Li  Li3  1  0.39000000  0.07000000  0.70000000  1
  Ge  Ge4  1  0.39000000  0.07000000  0.95000000  1
  Ge  Ge5  1  0.89000000  0.57000000  0.45000000  1
  F  F6  1  0.09000000  0.88000000  0.95000000  1
  F  F7  1  0.09000000  0.88000000  0.45000000  1
  F  F8  1  0.18000000  0.38000000  0.95000000  1
  F  F9  1  0.18000000  0.38000000  0.45000000  1
  F  F10  1  0.59000000  0.27000000  0.62000000  1
  F  F11  1  0.68000000  0.77000000  0.12000000  1
  F  F12  1  0.68000000  0.77000000  0.62000000  1
  F  F13  1  0.59000000  0.27000000  0.12000000  1
  F  F14  1  0.59000000  0.77000000  0.95000000  1
  F  F15  1  0.68000000  0.27000000  0.45000000  1
  F  F16  1  0.09000000  0.27000000  0.95000000  1
  F  F17  1  0.18000000  0.77000000  0.45000000  1
```

Figure 8: Cases of unconditional generation.

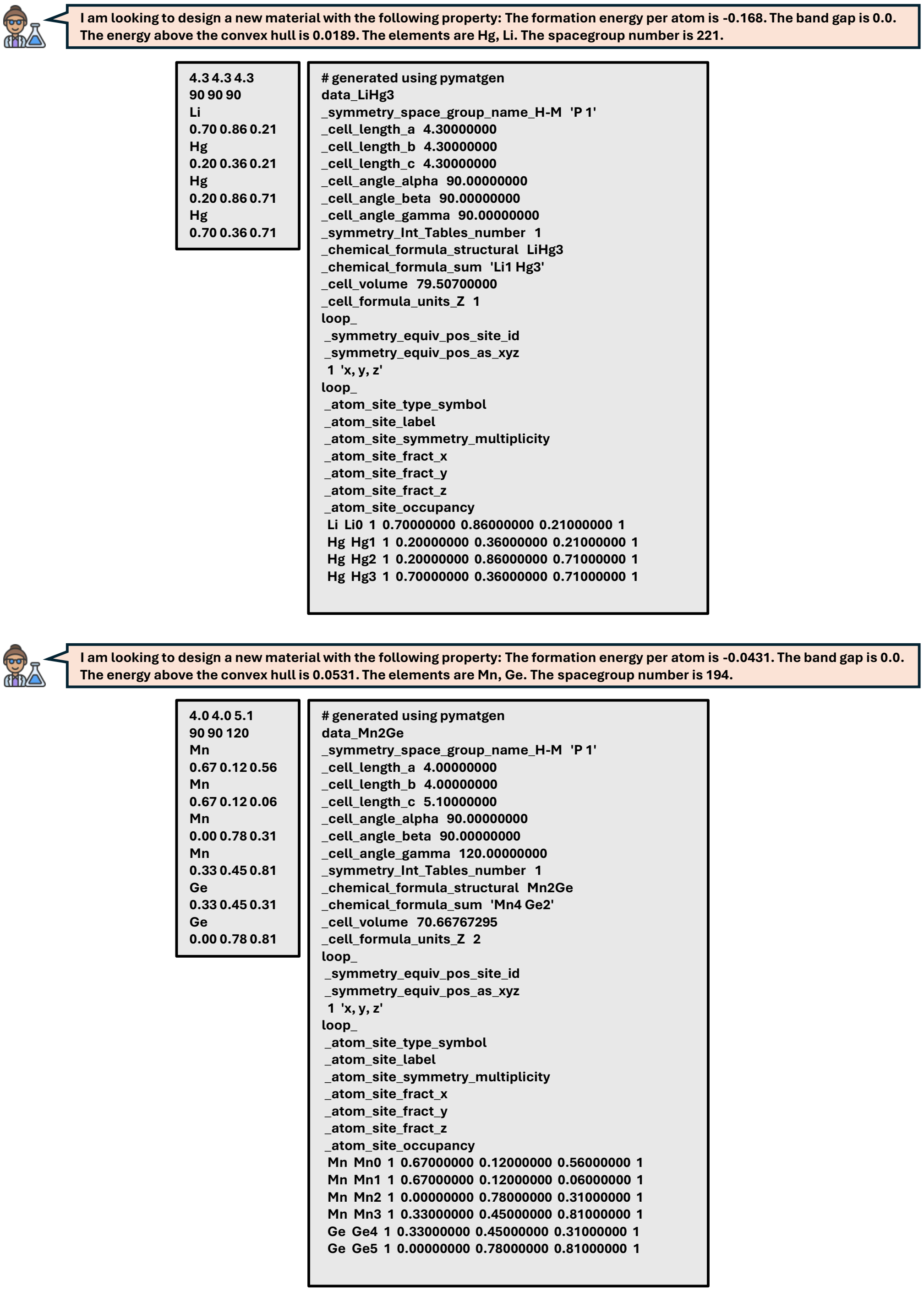

I am looking to design a new material with the following property: The formation energy per atom is -0.168. The band gap is 0.0. The energy above the convex hull is 0.0189. The elements are Hg, Li. The spacegroup number is 221.

```
4.3 4.3 4.3
90 90 90
Li
0.70 0.86 0.21
Hg
0.20 0.36 0.21
Hg
0.20 0.86 0.71
Hg
0.70 0.36 0.71
```

```
# generated using pymatgen
data_LiHg3
_symmetry_space_group_name_H-M  'P 1'
_cell_length_a  4.30000000
_cell_length_b  4.30000000
_cell_length_c  4.30000000
_cell_angle_alpha  90.00000000
_cell_angle_beta  90.00000000
_cell_angle_gamma  90.00000000
_symmetry_Int_Tables_number  1
_chemical_formula_structural  LiHg3
_chemical_formula_sum  'Li1 Hg3'
_cell_volume  79.50700000
_cell_formula_units_Z  1
loop_
 _symmetry_equiv_pos_site_id
 _symmetry_equiv_pos_as_xyz
  1  'x, y, z'
loop_
 _atom_site_type_symbol
 _atom_site_label
 _atom_site_symmetry_multiplicity
 _atom_site_fract_x
 _atom_site_fract_y
 _atom_site_fract_z
 _atom_site_occupancy
  Li  Li0  1  0.70000000  0.86000000  0.21000000  1
  Hg  Hg1  1  0.20000000  0.36000000  0.21000000  1
  Hg  Hg2  1  0.20000000  0.86000000  0.71000000  1
  Hg  Hg3  1  0.70000000  0.36000000  0.71000000  1
```

I am looking to design a new material with the following property: The formation energy per atom is -0.0431. The band gap is 0.0. The energy above the convex hull is 0.0531. The elements are Mn, Ge. The spacegroup number is 194.

```
4.0 4.0 5.1
90 90 120
Mn
0.67 0.12 0.56
Mn
0.67 0.12 0.06
Mn
0.00 0.78 0.31
Mn
0.33 0.45 0.81
Ge
0.33 0.45 0.31
Ge
0.00 0.78 0.81
```

```
# generated using pymatgen
data_Mn2Ge
_symmetry_space_group_name_H-M  'P 1'
_cell_length_a  4.00000000
_cell_length_b  4.00000000
_cell_length_c  5.10000000
_cell_angle_alpha  90.00000000
_cell_angle_beta  90.00000000
_cell_angle_gamma  120.00000000
_symmetry_Int_Tables_number  1
_chemical_formula_structural  Mn2Ge
_chemical_formula_sum  'Mn4 Ge2'
_cell_volume  70.66767295
_cell_formula_units_Z  2
loop_
 _symmetry_equiv_pos_site_id
 _symmetry_equiv_pos_as_xyz
  1  'x, y, z'
loop_
 _atom_site_type_symbol
 _atom_site_label
 _atom_site_symmetry_multiplicity
 _atom_site_fract_x
 _atom_site_fract_y
 _atom_site_fract_z
 _atom_site_occupancy
  Mn  Mn0  1  0.67000000  0.12000000  0.56000000  1
  Mn  Mn1  1  0.67000000  0.12000000  0.06000000  1
  Mn  Mn2  1  0.00000000  0.78000000  0.31000000  1
  Mn  Mn3  1  0.33000000  0.45000000  0.81000000  1
  Ge  Ge4  1  0.33000000  0.45000000  0.31000000  1
  Ge  Ge5  1  0.00000000  0.78000000  0.81000000  1
```

Figure 9: Cases of conditional generation.

Table 6: Numerical results of Ablation Study (Figure 6)

MatExpert	**- CoT Stage**	**- CoT Stage**	**- Retrieval Stage**
$\leq$ 5 atoms	76%	72%	62%
$\leq$ 10 atoms	69%	62%	59%
$\leq$ 25 atoms	66%	58%	51%
Space group	31%	30%	24%
Energy above hull	60%	56%	53%